



Congo red adsorption on shell powder and chitosan-coated shell powder biosorbents: experiments and theoretical calculation

Liu-Qin Ge, You-Zhou Zhou, Neng Fan, Mei-Sheng Xia*, Ling-Qing Dai, Ying Ye

Department of Marine Science, Ocean College, Zhejiang University, Zhoushan 316021, China, Tel. +86 13758246689; email: gliuqin@163.com (L.-Q. Ge), Tel. +86 18627953033; email: 21534038@zju.edu.cn (Y.-Z. Zhou), Tel. +86 17682300729; email: fanneng@zju.edu.cn (N. Fan), Tel. +86 580 2092326; email: msxia0201@163.com (M.-S. Xia), Tel. +86 18668431625; email: supermark_870625@hotmail.com (L.-Q. Dai), Tel. +86 580 2092306; email: gsyeying@zju.edu.cn (Y. Ye)

Received 5 March 2017; Accepted 17 June 2017

ABSTRACT

Shell powder (SP) with chitosan (CS) immobilized was applied as a composite biosorbent (CS-SP) for adsorptive removal of Congo red from aqueous solution. The materials were characterized using Fourier transform infrared spectroscopy, X-ray diffraction, and scanning electron microscopy. Dye adsorption onto SP and CS-SP was investigated under varied conditions such as chitosan content, initial dye concentration, pH, salt concentration, and temperature. The optimum CS content was determined as 15 wt%, under which CS-SP displayed a fine coating structure and a greater adsorption capacity of 258.53 mg/g compared with 36.50 mg/g for SP at 30°C. The composite adsorbent maintained its performance in high-salinity, acidic or alkaline environment, and exhibited excellent reusability throughout five-recycle regeneration. The dynamic data conformed to pseudo-second-order and Elovich models while the equilibrium isotherms followed Langmuir and Temkin models, which revealed that chemisorption was involved in the adsorption mechanism. Besides, the maximum monolayer adsorption capacity for CS-SP reached 263.85, 283.29, 322.58 mg/g at 30°C, 40°C, and 50°C, respectively, and adsorption on CS-SP was verified to be endothermic and spontaneous from thermodynamic study. The results indicated that the prepared CS-SP biosorbent is quite promising for dye wastewater treatment.

Keywords: Shellfish shell; Chitosan; Biosorbent; Congo red; Adsorption

1. Introduction

Nowadays, extensive use of dyes in textile, plastic, leather, paper, and related industries has produced large volumes of dye wastewater. Most dyes are toxic, non-biodegradable, carcinogenic and mutagenic for human being and aquatic life [1]. For example, Congo red (CR), a common benzidine-based anionic diazo dye, has been ascertained to cause allergic responses and to be metabolized to benzidine, known as a human carcinogen [2–4]. Therefore, dyes are among the most hazardous substances existing in industrial effluents, and the wastewater treatment issue should be taken seriously ahead of

discharge [5]. In order to remove dye contaminations, a variety of techniques have been employed, such as coagulation and flocculation [6], membrane process [7], photocatalytic degradation [8], biological treatment [9], and adsorption [10,11]. Majority of these methods display a high expense or poor effectiveness, whereas adsorption is typically considered as an attractive process with advantages of simple operation, easy recovery, high efficiency and low cost as well.

The exploration of environment-friendly natural biosorbents, for example, rice husk [12], cotton [13], *Hibiscus cannabinus* fiber [14], de-oiled soya [15], egg shell [16], hen feather [17], and chitosan [18], has attracted growing interest. However, more noteworthy are composite biosorbents like iron oxide-impregnated

* Corresponding author.

dextrin [19], montmorillonite-immobilized alginate [20] and alginate/Fe₃O₄ nanocomposite [21] for their outstanding comprehensive properties. The polyaminosaccharide chitosan (CS) is derived from partial N-deacetylation of chitin, the second most abundant biopolymer in nature due to its wide distribution in crustaceans, insects, fungi, etc. Owing to multiple functional groups (–NH₂, –OH), as well as biocompatibility, biodegradability, and non-toxicity [22], CS has exhibited an excellent adsorbability and potential for dye removal. Nevertheless, CS also exposed the disadvantages of low specific gravity, poor mechanical strength, and acid instability [1]. To pave the way for its widespread application, strenuous efforts have been endeavored by immobilization of CS on rigid inorganic materials to prepare CS composites [23], most of which are synthesized by CS precipitation from its acid solution onto the inorganic substance under pH adjustment [24,25]. In previous studies, CS has been immobilized on various sorts of materials, such as clay [24], quartz sand [26], hydroxyapatite [1], and magnetic iron oxide. However, due to incompatibility between CS and the inorganics, those resulted composites may suffer from poor interfacial adhesion which adversely affected their adsorption performance [26]. Organo-modification to the inorganic substance could improve its compatibility with CS and thus enhance the adsorption capacity [27], but inevitably complicates preparation procedures.

Shells, a kind of by-products generated from worldwide shellfish cultivation, have been listed as one of the most serious environmental issues due to disposing difficulty [28]. The shell belongs to biominerals, and as distinct from mine calcium carbonate, it contains about 95% calcium carbonate and 5% biomacromolecules including proteins, polysaccharides, and glycoproteins [29], making it a natural organic/inorganic composite. It has been confirmed that shell powder (SP) surface possesses a variety of functional groups [30] such as amino (–NH₂), hydroxyl (–OH), and carboxyl (–COOH), which impart inherent organic affinity to SP [31]. Although shell waste has been successfully applied to polymer fillers and many other fields [32], its application in adsorption is sparse, except for desulfurization, denitrification, and phosphate removal after thermal treatment of calcination and pyrolysis [32].

Thus, in this paper, the natural structure of SP was retained and utilized to prepare a chitosan-coated shell powder (CS-SP) composite biosorbent, and the obtained adsorbent was then adopted for CR removal from aqueous solution. Operation parameters including chitosan content in CS-SP, adsorbent dosage, initial pH, salt concentration, and temperature were investigated in detail. The adsorption dynamics, isotherms, thermodynamics as well as adsorbent recycle were also researched.

2. Experimental procedure

2.1. Materials

SP was prepared from pearl shell [28] supplied by a food factory in Changzhou, China. CR (purity >98%) was purchased from Aladdin Biochemical Technology Co., Ltd. (Shanghai, China). Chitosan (BR), hydrochloric acid (AR), sodium hydroxide (AR), sodium chloride (AR), and sodium

sulfate (AR) were all bought from Sinopharm Chemical Reagent Co., Ltd. (Shanghai, China). All the reagents were used without further purification.

2.2. Preparation of chitosan-coated shell powder

CS-SP composite was fabricated through the simple method of liquid phase deposition [24,25]. CS was first dissolved in diluted hydrochloric acid of 0.1 mol/L to prepare 1 wt% CS solution, while SP were dispersed uniformly into deionized water with the mass ratio of 1:60 through stirring. After that, the CS solution was added dropwise into SP suspension under 900 rpm mixing speed, during which CS was precipitated on SP. After CS addition, the resulted mixed system was filtered by means of bolting silk with 250 mesh size, then the filter residue was rinsed with deionized water under the mass ratio of 40:1, dried at 50°C for 24 h and finally ground into granules to obtain CS-SP. In this work, different additive amount of CS in SP was studied, including 0, 5, 10, 15, 20, and 25 wt%, and the prepared adsorbents were named as SP, 5%, 10%, 15%, 20%, and 25% CS-SP, respectively.

2.3. Characterization

Infrared spectra of SP and CS-SP were measured using a Nicolet 560 Fourier Transform Infrared Spectroscopy (FTIR) Instrumentation by potassium bromide disc method. The crystalline phases present in the samples were identified by a Shimadzu X-ray diffractometer (XRD-6000) at 40 kV and 40 mA, with a Cu K α radiation source, and 2 θ scale range of 10°–80°. Besides, morphologies of SP and CS-SP were observed by scanning electron microscopy (SEM) in a Hitachi SU8000 field emission SEM at a voltage of 3 kV. Prior to inspection, the samples were sputter-loaded with platinum.

2.4. Adsorption experiment

The CR adsorption experiments were carried out by agitating 0.06 g of the adsorbent with 30 mL of dye solution for 10 h at 200 rpm and 30°C, in a thermostated rotary shaker (Hualida, HZ-9210K, Taicang, China). During a saturated adsorption study, the adsorption performances of CS-SP with different chitosan content were compared with each other to confirm the optimal additive amount. Effect of adsorbent dosage was investigated with different adsorbent doses (0.01–0.12 g) and 30 mL of 400 mg/L dye solutions. In the pH effect experiment, initial pH values of the solution (400 mg/L) were adjusted to 3.40–10.88 using dilute HCl or NaOH solution. To evaluate the salt influence, sodium chloride or sodium sulfate (0.025–0.3 mol/L) was added to the dye solution (400 mg/L) for dye effluent simulation. Moreover, adsorption dynamics, isotherms, and thermodynamics were researched under various temperature conditions (30°C, 40°C, and 50°C). The above studies were carried out for SP and CS-SP simultaneously. After adsorption for the desired time, the treated dye solution was separated from the adsorbent in a centrifuge (Eppendorf, 5804, Germany) at 10,000 rpm for 3 min. Dye concentration was then estimated by monitoring the absorbance at 496 nm using a UV-Vis spectrophotometer (Shimadzu, UV-2550, Tokyo, Japan). All the experiments were carried out in triplicates, and

the reported values were obtained by averaging the three data sets. Adsorptive removal of CR from the solution was evaluated by the amount of adsorption (q_e , mg/g) and percentage removal (% removal).

3. Results and discussion

3.1. Characterization

As can be seen from the IR spectra (Fig. 1(a)), the spectrograms of SP, 5%, 15%, and 25% CS-SP were identical in peak positions. The bands located at 715, 870, 1,078, and 1,426 cm^{-1} were attributed to the in-plane bending

vibration, out-of-plane bending vibration, symmetric stretch, and asymmetric stretch of CO_3^{2-} [33], respectively. In accordance with previous research [30], the presence of organic matters on SP was verified from the IR spectra. The peak at 2,892 cm^{-1} belonged to stretching vibration of CH, and the band at 3,428 cm^{-1} was ascribed to the –OH and –NH stretching [22,30]. Considering the intensity of carbonate peak (1,426 cm^{-1}) as contrast, an obviously enhancing trend could be found in the organic peak intensity of SP, 5%, 15%, and 25% CS-SP, being a result of the increase in CS content. Benefited from the surface characteristic of SP, it was likely to immobilize CS on it to further improve its surface activity along with application performance in dye adsorption. As revealed from

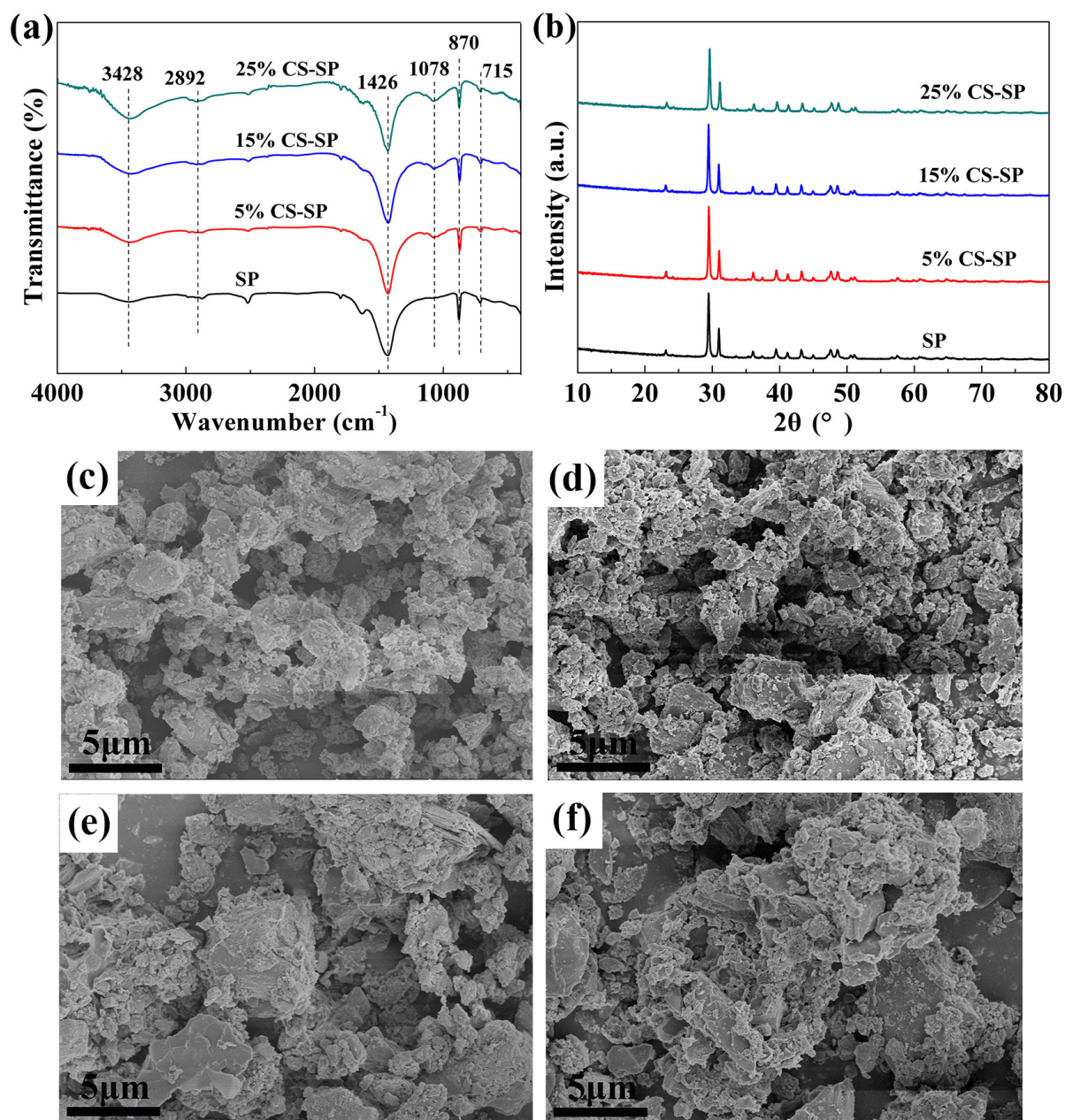


Fig. 1. Characterizations of shell powder (SP) and chitosan-coated shell powder (CS-SP): (a) FTIR spectra; (b) XRD patterns; SEM image of (c) SP, (d) 5% CS-SP, (e) 15% CS-SP, and (f) 25% CS-SP.

the X-ray diffraction (XRD) patterns (Fig. 1(b)), all the main crystalline phases presented in samples were calcite, indicating that the introduced CS did not crystallize independently but closely attached to the SP particles.

The microstructures of SP and CS-SP were displayed in the SEM images (Figs. 1(c)–(f)). From Figs. 1(c) and (d), it can be seen that similarly to unmodified-SP, a large number of SP surfaces in 5% CS-SP were still exposed, demonstrating that the 5 wt% additive amount was not enough to make coating achieved. With the increase in CS content, coating layers gradually got formed and it was finally obtained at 15 wt% content as confirmed in Fig. 1(e). The successful coating could be ascribed to the inherent organic affinity of SP with distinctive surface characteristics [30], which contributed to producing strong interfacial adhesion between SP and CS. When CS content became much higher, agglomeration occurred among different particles resulted from the physical crosslinking of CS molecules (Fig. 1(f)).

3.2. Effect of CS content on adsorption

The CR adsorption on SP and CS-SP with different CS content was measured in the same gradient of initial dye concentration, so as to seek out the optimal CS

additive amount. As presented in Fig. 2(a), with the raised CR concentration, the adsorption quantities of all the adsorbents kept increasing till reaching ultimate values. At low content ($\leq 15\%$), the adsorption capacity was significantly enhanced by raised CS percentage, while at high content ($>15\%$), the enhancement tended to be unobvious. Remarkably, the adsorption capacity of 15% CS-SP was nearly six times higher than that of SP, and this great improvement was due to the excellent CR adsorption performance of CS. In aqueous solution, the amine groups ($-\text{NH}_2$) on CS were protonated to form cations ($-\text{NH}_3^+$) while CR molecules ionized to generate negative ions (SO_3^-), thus adsorption was enhanced as a result of strong electrostatic attractions between them [34].

As discussed in the SEM results, SP particles were not well-coated until the CS content reached 15 wt%. Consequently, addition of CS below 15 wt% decreased the uncovered surfaces of SP, and noticeably increased the adsorption capacity. When content was higher than 15 wt%, the already formed CS coating and emerging particle agglomeration jointly reduced the modification effect and limited the continuing enhancement in adsorption. It was finalized that the optimal additive amount of CS was 15 wt% in this work. Therefore, the subsequent experiment was conducted on SP and 15% CS-SP, and the 15% CS-SP adsorbent was hereafter named as CS-SP.

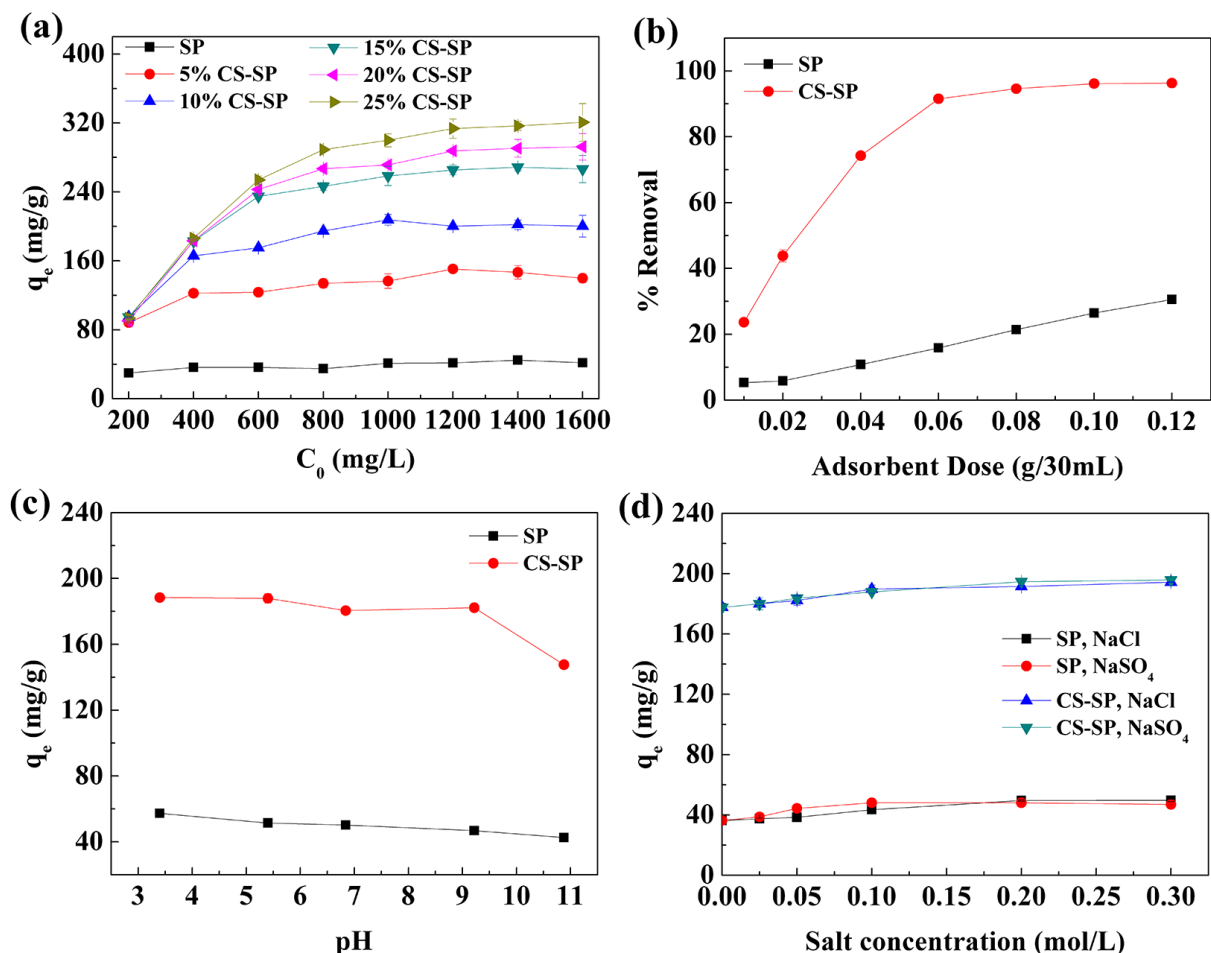


Fig. 2. Variation in adsorption with different process parameters: (a) CS content; (b) adsorbent dosage; (c) solution pH; (d) salt concentration.

3.3. Effect of adsorbent dosage

Fig. 2(b) presented the removal of CR by SP and CS-SP under different adsorbent dosage (0.01–0.12 g/30 mL) at the dye concentration of 400 mg/L. The removal efficiency by CS-SP was enhanced significantly with increase in adsorbent addition with the dose lower than 0.06 g/30 mL, while the removal rate almost reached a plateau (larger than 90%) when adding more CS-SP adsorbent. The maximum removal efficiency obtained was higher than 96%. As to SP, the percentage removal kept gradually rising but lower than 30% within the whole experimental range. Accordingly, the adsorbent dosage in this work was chosen as 0.06 g/30 mL, and SP was used as a contrast under the same dose.

3.4. Effect of pH

The effect of initial pH (3.40–10.88) of the dye solution (400 mg/L) was shown in Fig. 2(c). With the increase in pH value, it can be seen that both of SP and CS-SP exhibited slight downward trends in the adsorption capacity.

The pH effect could be ascribed to the electrostatic interaction between the dye and adsorbents. The point of zero charge (pH_{PZC}) of SP and CS-SP were obtained at 9.95 and 9.83, respectively, by the method of potentiometric titration [35,36]. The relatively high adsorption observed at low pH values ($\text{pH} < \text{pH}_{\text{PZC}}$) was partially due to strong electrostatic attraction between positively charged surface of the adsorbents and negatively charged CR molecules. In addition, surface dissolution of the adsorbents in acidic solution enlarged the specific surface area, which contributed to adsorption improvement as well. With increase of the pH values, adsorption decreased owing to the weakened electrostatic attraction resulted from reduced positive charge on adsorbents, as well as the presence of abundant OH^- ions in solution competing with the anionic dye for adsorption sites. As discussed therein before, the electrostatic interactions between dye and CS-SP was mainly caused by the protonation of amine groups on CS. As a result, caused by the large reduction of protonation in CS [34], adsorption on CS-SP suddenly declined when $\text{pH} > 9.22$.

However, there was still significant adsorption observed in alkaline solution even when $\text{pH} = 10.88$, indicating an existence of other pathways for CR adsorption. Similarly to CS with rich amino and hydroxyl groups, in CR there also existed O, N, and S atoms that can form quantities of hydrogen bonds with CS-SP adsorbent [37]. Furthermore, except the above mechanisms, it was supposed that additional ways like chemisorption probably existed, which was supported by the adsorption on SP in alkaline pH. It was worth mentioning that CS-SP adsorbent in this work was applicable to a wide pH range especially acidic condition. The commendable acid stability was ascribed to the strong interfacial adhesion between SP and CS, as well as acid neutralization by the SP component.

3.5. Effect of salts concentration

Sodium salt is often used as a stimulator in dye industries, and the discharged wastewater consequently contains high concentration of salts [37], which may affect the adsorption removal efficiency. In this paper, salt influences from sodium

chloride and sodium sulfate were investigated at the initial CR concentration of 400 mg/L (Fig. 2(d)). With addition of the two salts, no reduction but a little improvement in adsorption performance was observed. It can be explicable that salts may shield the electrostatic attraction between opposite charges and decrease the repulsion of the same charges in adsorbents and the dye molecules [25]. Since both of the salts showed no adverse effects on the CR adsorption, the adsorbents were expected to be broadly utilized in high-salinity environment.

3.6. Adsorption dynamics

The adsorption of CR (400 mg/L) onto SP and CS-SP at a series of time and temperature (30°C, 40°C, 50°C) was presented in Fig. 3(a). At this initial dye concentration, there was no obvious difference in adsorption dynamics under three temperatures, but the equilibrium capacity for CS-SP was much higher than that for SP. The adsorption on CS-SP could be easily divided into two stages: increment in adsorption amount was found to be significant during the first 90 min, then it started to slow down and equilibrium was attained after 360 min. As for SP, the equilibrium was faster reached in 120 min. Five kinetic models, that is, pseudo-first-order equation [38], pseudo-second-order equation [39], liquid-film diffusion [40], Elovich equation [41], and intra-particle diffusion equation [42] were adopted to investigate the kinetics of CR adsorption at 30°C and to determine controlling mechanisms of the adsorption process. The fitting curves were presented in Figs. 3(b)–(f).

The pseudo-first-order and pseudo-second-order equations are expressed as Eqs. (1) and (2), respectively.

$$\ln(q_e - q_t) = \ln q_e - k_1 t \quad (1)$$

$$\frac{t}{q_t} = \frac{1}{k_2 q_e^2} + \frac{t}{q_e} \quad (2)$$

where q_e and q_t (mg/g), respectively, are the amount of CR adsorbed on adsorbents at equilibrium and at time t (min), k_1 (min^{-1}) is the pseudo-first-order rate parameter and k_2 ($\text{g}/(\text{mg min})$) is the pseudo-second-order rate parameter.

As can be seen from Figs. 3(b) and (c), for both adsorption on SP and CS-SP, the pseudo-first-order model did not match well with the experimental data (correlation coefficient $R^2 < 0.80$), while the pseudo-second-order model provided an excellent fit ($R^2 > 0.99$) and the calculated equilibrium adsorption capacities ($q_{e(\text{cal}, \text{SP})} = 41.12$ mg/g, $q_{e(\text{cal}, \text{CS-SP})} = 186.22$ mg/g) were quite compatible with the experimental values ($q_{e(\text{exp}, \text{SP})} = 40.99$ mg/g, $q_{e(\text{exp}, \text{CS-SP})} = 182.76$ mg/g). The results indicated that chemisorption might be a rate-controlling step in the adsorption process [43,44].

The liquid-film diffusion model is given as Eqs. (3) and (4):

$$-\ln(1 - F) = k_{\text{fd}} t \quad (3)$$

$$F = \frac{q_t}{q_e} \quad (4)$$

where F is fractional attainment of equilibrium at time t and k_{fd} (min^{-1}) is the adsorption rate constant. It was indicated from Fig. 3(d) that the liquid-film diffusion model was not suitable for the entire adsorption process ($R^2 < 0.87$). However, there were linear relations before 20 min for SP and 90 min

for CS-SP, verifying fitness of this model and domination of liquid-film diffusion in the beginning stage.

The Elovich model has been widely used to describe chemical adsorption kinetics [43,45], and the model is shown in Eq. (5):

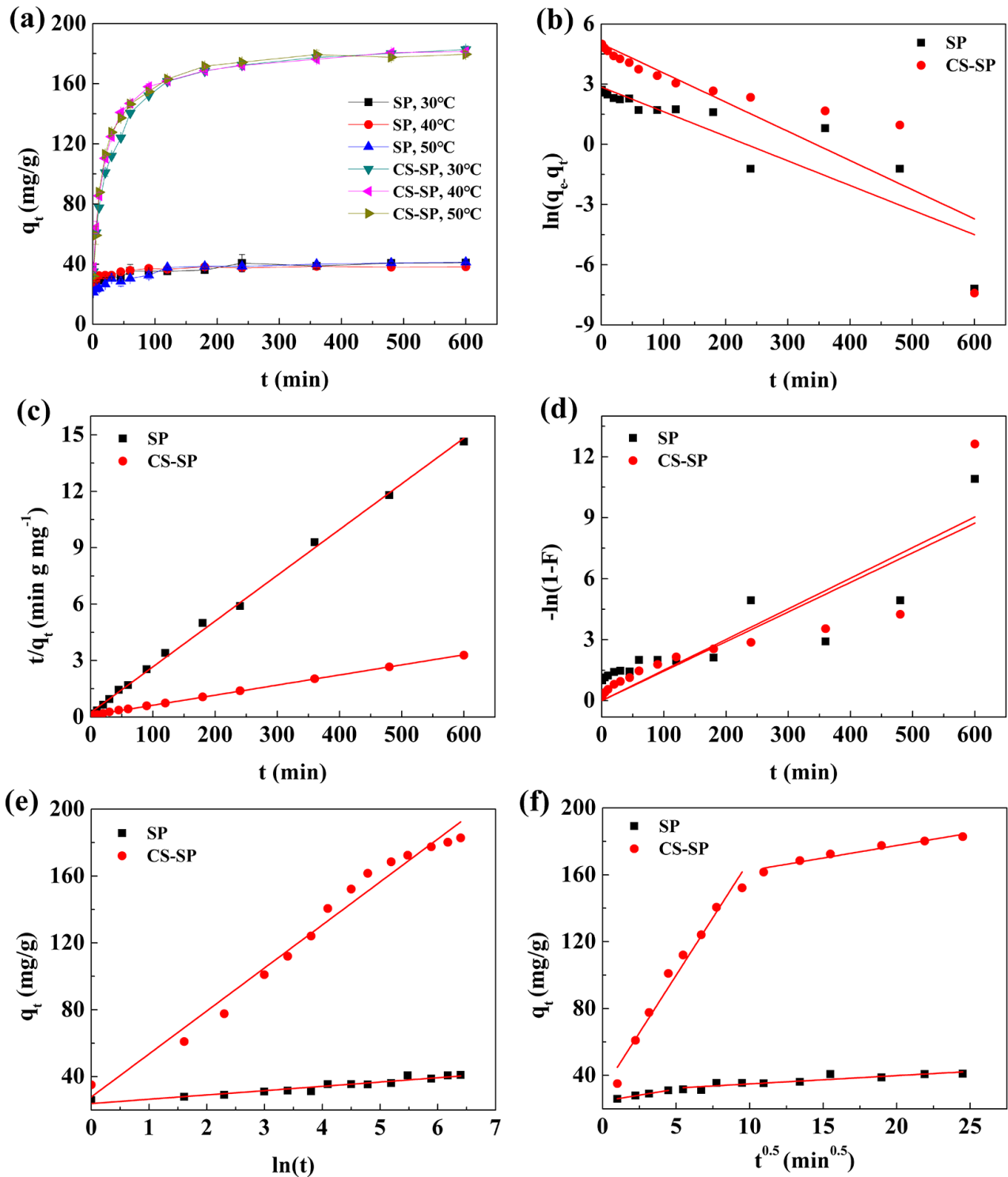


Fig. 3. Adsorption dynamics: (a) adsorption capacity at different time and temperature; linear fitting by kinetic models of (b) Pseudo-first-order, (c) Pseudo-second-order, (d) Liquid-film diffusion, (e) Elovich, and (f) Intra-particle diffusion.

$$q_t = \frac{1}{\beta} \ln(\alpha\beta) + \frac{1}{\beta} \ln t \quad (5)$$

where α (mg/g min) is the initial adsorption rate constant, β (g/mg) is a constant related to the surface coverage and the activation energy for chemical adsorption. As shown in Fig. 3(e), the CR adsorption onto SP and CS-SP can be described by the Elovich model ($R^2_{SP} = 0.9164$, $R^2_{CS-SP} = 0.9755$), and in accordance with pseudo-second-order modeling, this result demonstrated the existence of chemisorption as well.

The intra-particle diffusion model is described as Eq. (6):

$$q_t = k_{id} t^{0.5} + C \quad (6)$$

where k_{id} is the intra-particle diffusion rate constant ($\text{mg/g min}^{-0.5}$) and C (mg/g) is associated with the extent of boundary layer effect. As can be seen from Fig. 3(f), the intra-particle diffusion model did not fit the data throughout the experiment, while multi-linearity could be obtained particularly for CS-SP, indicating that the adsorption process was not governed by a single step [46].

In summary, the adsorption mechanisms on SP and CS-SP were proposed as follows. At the initial 20 min for SP and 90 min for CS-SP, external diffusion or boundary layer diffusion of adsorbate molecules was the rate-limiting step, which could be confirmed from the liquid-film diffusion modeling. In this period, CR molecules diffused from solution and through liquid film to the external CS surface of adsorbents. The second stage for CS-SP was more gradual and governed by internal or intra-particle diffusion, where CR molecules were transferred through CS coating to be adsorbed onto site of the inner SP surface. As to SP, the adsorbate was directly adsorbed during the second phase without an internal diffusion. Throughout the process, CR was adsorbed in several pathways, including electrostatic interaction between the adsorbate and adsorbents along with hydrogen bonding between CR and CS. Furthermore, chemisorption could not be neglected based on the above results, and the probable interpretation was raised hereinafter. In aqueous solution, CR dye was ionized to generate negative ions (SO^{3-}), and calcium sulfonate was produced on adsorbents through chemical reaction between SO^{3-} and CaCO_3 (Fig. 4).

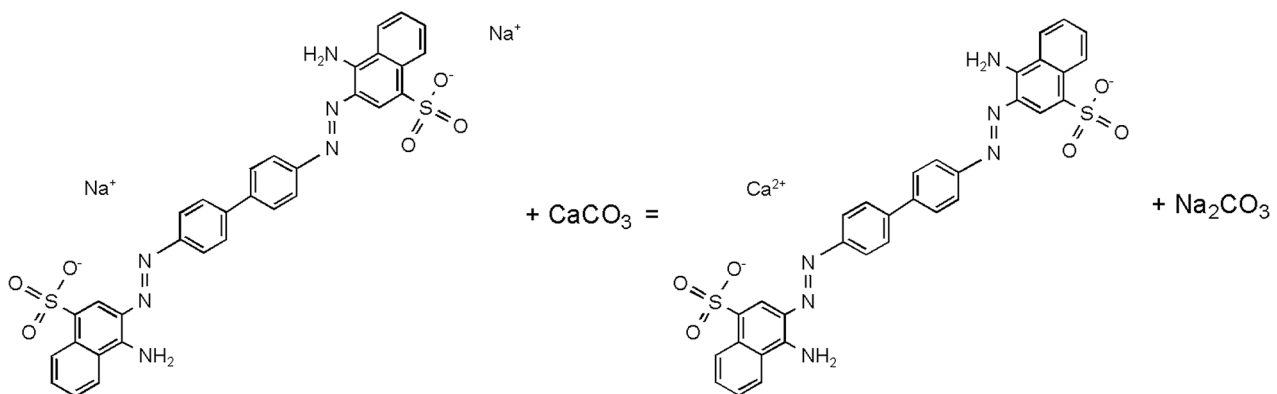


Fig. 4. The possible chemical reaction between CR and adsorbents.

3.7. Adsorption isotherms

The adsorption isotherms at different temperatures were shown in Fig. 5(a). As compared with SP, adsorption on CS-SP was obviously improved by temperature increase especially in high initial CR concentrations. The temperature effect was ascribed to the facilitated internal diffusion on CS-SP, a result synergistically affected by promotion in diffusivity of the dye molecule and increment in the pore size of CS coating [3]. Four adsorption isotherm models, including Langmuir [47], Freundlich [48], Temkin [49], and Dubinin-Radushkevich (D-R) [50] models, were then introduced to explore the equilibrium adsorption. The fitting curves were presented in Figs. 5(b)–(e), and some of the calculated parameters shown in Table 1.

The Langmuir and Freundlich equations are two widely employed adsorption isotherm models. Langmuir model is based on the assumption that monolayer adsorption occurred over an adsorbent surface with homogenous sorption energies and no interaction between the adsorbed molecules was included. In contrast, Freundlich model considered multilayer adsorption on a heterogeneous adsorbent surface accompanied by interaction between adsorptive molecules. The Langmuir and Freundlich models can be expressed as Eqs. (7) and (8), respectively.

$$\frac{C_e}{q_e} = \frac{1}{q_m b} + \frac{1}{q_m} C_e \quad (7)$$

$$\ln q_e = \ln K_f + \frac{1}{n} \ln C_e \quad (8)$$

where C_e is the equilibrium concentration of the adsorbate (mg/L), q_e is the adsorption capacity at equilibrium (mg/g), q_m (mg/g) is the maximum adsorption capacity calculated, b (L/mg) is the Langmuir constant related to the adsorption energy, and K_f ($(\text{mg/g}) (\text{L/mg})^{1/n}$) and n are Freundlich constants associated to the adsorption capacity and adsorption intensity, respectively. Figs. 5(b) and (c) and Table 1 show that the experimental data followed well with the Langmuir model, but did not accord with the Freundlich model. The maximum monolayer adsorption capacities calculated from Langmuir model are presented in Table 1.

The Temkin isotherm is assumed that the adsorption heat decreases linearly with coverage due to adsorbate/adsorbate interactions, and it has the form as Eq. 9:

$$q_e = \frac{RT \ln A_T}{b_T} + \frac{RT}{b_T} \ln C_e \quad (9)$$

where A_T is the Temkin isotherm equilibrium binding constant (mg/L), b_T is related to adsorption heat (J g/(mg mol)), R is the gas constant (8.314 J/(mol K)), and T is the absolute temperature (K). As shown in Fig. 5(d) and Table 1, the present work data for CS-SP were fitted well to the Temkin model, which further proved the presence of a chemical adsorption [51] on CS-SP. The fitting signature for CS-SP was better

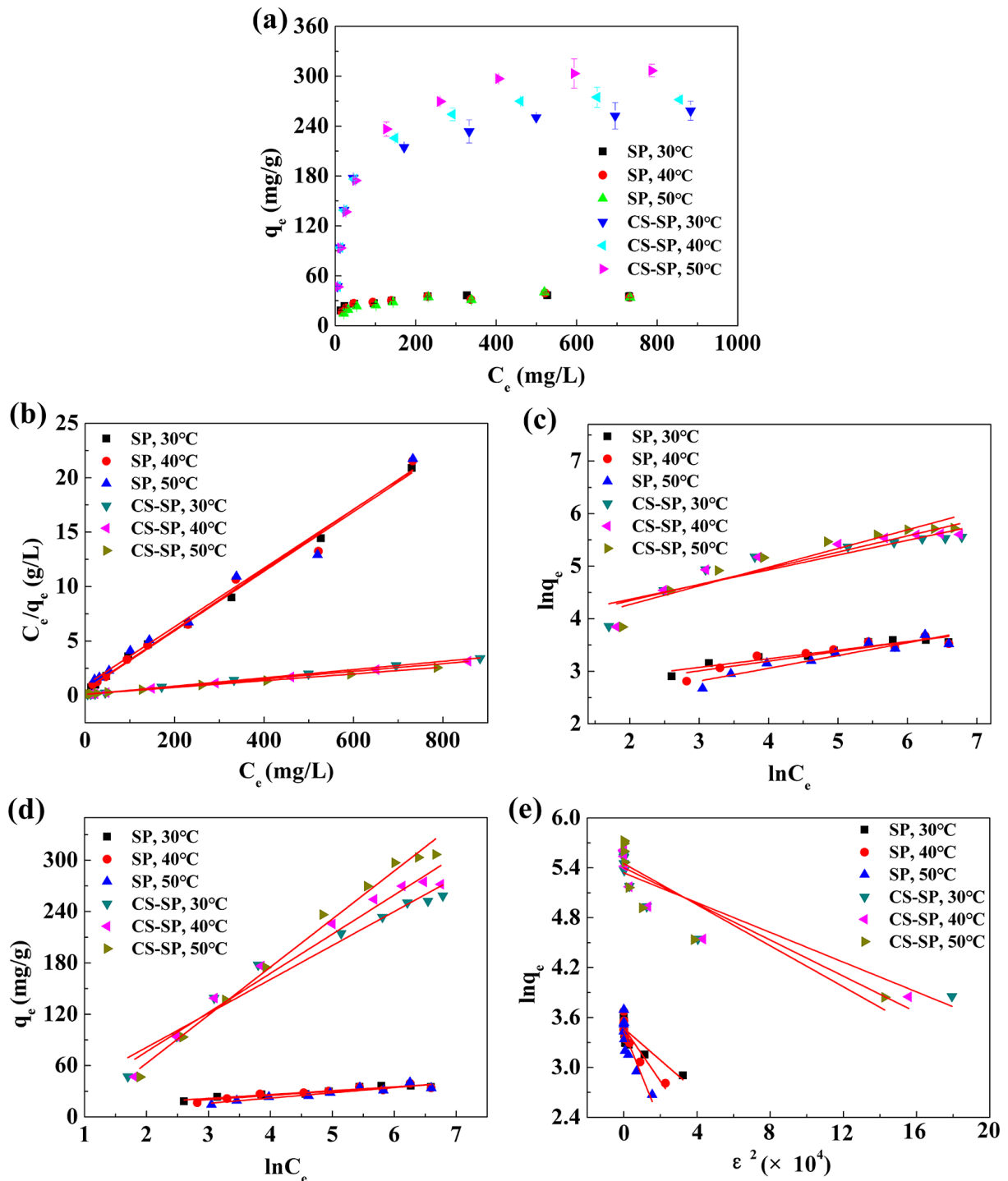


Fig. 5. Equilibrium adsorption at different temperature: (a) adsorption isotherms; linear fitting by isotherm models of (b) Langmuir, (c) Freundlich, (d) Temkin, and (e) D–R.

Table 1

Parameters of adsorption isotherm models for CR adsorption onto SP and CS-SP at different temperatures (30°C, 40°C, and 50°C)

Isotherms/constants	SP, 30°C	SP, 40°C	SP, 50°C	CS-SP, 30°C	CS-SP, 40°C	CS-SP, 50°C
Langmuir						
q_m (exp, mg/g)	36.50	35.21	34.43	258.53	274.74	306.85
q_m (cal, mg/g)	36.58	36.28	37.09	263.85	283.29	322.58
b , L/mg	0.0568	0.0515	0.0292	0.0369	0.0354	0.0250
R^2	0.9968	0.9869	0.9793	0.9992	0.9995	0.9995
Freundlich						
R^2	0.8925	0.8182	0.8667	0.8293	0.8446	0.8887
Temkin						
A_T , mg/L	6.137	3.076	0.669	1.050	0.716	0.414
b_T , J g/(mg mol)	560.56	529.65	437.40	63.49	56.86	47.82
R^2	0.9071	0.8399	0.8653	0.9591	0.9682	0.9879
D–R						
R^2	0.7161	0.8167	0.7627	0.8122	0.8223	0.7712

than that for SP, which was also observed in kinetic study of pseudo-second-order and Elovich equations. The distinction in model fitting could be put down to the high adsorption capacity of CS-SP that made more chemisorption occurred on it.

The D–R model, an equation often adopted to distinguish between physical adsorption and chemical adsorption [52], is given as Eqs. (10) and (11):

$$\ln q_e = \ln q_m - B\varepsilon^2 \quad (10)$$

$$\varepsilon = RT \ln \left(1 + \frac{1}{C_e} \right) \quad (11)$$

where q_m is the D–R adsorption capacity (mg/g), B is the activity coefficient related to the mean adsorption energy (mol^2/J^2), and ε is the Polanyi potential. The results (Fig. 5(e) and Table 1) illustrate a poor correlation between the experimental data and this model, according with the adsorption mechanisms of physisorption accompanied with chemisorption in this work.

As a new composite biosorbent, the developed CS-SP adsorbent exhibited a relatively high adsorption performance for CR when compared with previously reported CS composites (Table 2). The adsorption capacity of CS-SP was even higher than that of graphene oxide/CS fiber [52], and comparable with CS/organo-montmorillonite nanocomposite [27]. The much higher adsorption on CS/organo-montmorillonite compared with that on CS/montmorillonite could be due to the improved compatibility and interfacial adhesion between CS and montmorillonite resulted from organic modification [27,53]. As to SP, benefited from its inherent organic affinity [30], reasonable adsorbability was obtained on well-coated CS-SP (section 3.1.). Significantly large adsorption capacity was observed on CS/carbon nanotube for its nanostructure [54], and on hydroxyapatite/CS composite mainly because of its extremely high CS content (50 wt%) [1]. By virtue of the abundant shellfish shell resource and simple

Table 2

Comparison between maximum adsorption capacities (q_m) of various CS composites calculated from Langmuir model for CR adsorption

Adsorbents	q_m , mg/g	References
CS-coated quartz sand	4	[26]
CS-coated magnetic iron oxide	43	[25]
CS/montmorillonite	55	[53]
CS-alginate sponge	122	[55]
Graphene oxide/CS fiber	227	[52]
CS/organo-montmorillonite	291	[27]
CS/carbon nanotubes	450	[54]
Hydroxyapatite/CS	769	[1]
CS-SP	264	This work

preparation process, utilization of CS-SP for dye removal was expected to be more economical than those adsorbents like CS/organo-montmorillonite, graphene oxide/CS fiber and CS/carbon nanotube.

3.8. Adsorption thermodynamics

Considering the obvious temperature effect on CR adsorption onto CS-SP, it is necessary to further study its thermodynamic parameters, including the change of standard Gibbs free energy change (ΔG^0), change of standard enthalpy (ΔH^0), and change of standard entropy (ΔS^0), which can be determined by the following equations [56]:

$$\Delta G^0 = -RT \ln K_c \quad (12)$$

$$\ln K_c = \frac{\Delta S^0}{R} - \frac{\Delta H^0}{RT} \quad (13)$$

$$K_c = \frac{C_s}{C_e} \quad (14)$$

Table 3
Thermodynamic parameters for the adsorption of CR onto CS-SP

C_0 , mg/L	ΔH^0 , kJ/mol	ΔS^0 , J/(mol K)	ΔG^0 , kJ/mol		
			30°C	40°C	50°C
600	16.05	112.24	-17.98	-19.07	-20.23
800	15.80	106.67	-16.52	-17.63	-18.65
1,000	15.35	102.22	-15.67	-16.60	-17.72
1,200	13.91	94.82	-14.86	-15.74	-16.76
1,400	11.64	85.44	-14.31	-15.00	-16.03
Mean	14.55	100.28	-15.87	-16.81	-17.88

where K_c is adsorption equilibrium constant or distribution coefficient, C_s is the amount of CR adsorbed per mass of adsorbent (mg/g), C_e is the CR concentration in solution at equilibrium (mg/mL), R is the gas constant (8.314 J/(mol K)), and T is the absolute temperature (K).

In this paper, the thermodynamic parameters of adsorption on CS-SP were calculated from the experimental data with $C_0 \geq 600$ mg/L, since temperature influence was remarkable at high concentrations. As shown in Table 3, the negative values of ΔG^0 demonstrated the spontaneous nature of CR adsorption onto CS-SP and feasibility of the dye removal process within 30°C–50°C range. Increased absolute value of ΔG^0 with the rise of temperature revealed the higher affinity and favorability of CR adsorption onto CS-SP at higher temperature. The positive values of ΔH^0 confirmed the endothermic nature of the adsorption process, which was consistent with the increased adsorption of CR at high temperature. The endothermal characteristic of CR adsorption was also discovered in relevant studies about chitosan composites such as chitosan-coated magnetic iron oxide [25] and hydroxyapatite/CS composite [1]. Moreover, the positive ΔS^0 reflected an incremental randomness at the solid–solution interface during adsorption.

3.9. Recycling of CS-SP adsorbent

The regeneration performance of the CS-SP biosorbent was investigated to evaluate its industrial applicability. Dye-adsorbed CS-SP was first eluted by mixture solution of NaOH (0.1 mol/L) and ethanol with the volume ratio of 1:1, then washed with deionized water. After desorption, the adsorbent was dried and ground, then used to remove CR (400 mg/L) in another cycle. An excellent reusability was displayed from the experimental result that the adsorption capacity in five adsorption–desorption cycles was 180.5, 180.1, 179.0, 178.4, and 177.5 mg/g, respectively. This confirmed a sufficient stability of the coating structure on CS-SP, which could be attributed to the strong interfacial adhesion between CS and SP.

4. Conclusions

A novel CS-SP biosorbent was obtained at chitosan (CS) content of 15 wt%. Adsorption experiments toward CR revealed that CS-SP adsorbent had an improved adsorption capacity six times higher than that of SP. The biosorbent was reusable, and adaptable to high-salinity, acidic or alkaline environment. The adsorption behavior, in which

electrostatic interaction, hydrogen bonding, and chemisorption was included, was well fitted with pseudo-second-order and Langmuir models, and moreover, verified to be endothermic and spontaneous. This research proposed a promising biosorbent for dye wastewater treatment and also contributed to resource utilization of shellfish shell waste.

Symbols

A_T	–	Temkin isotherm equilibrium binding constant, mg/L
B	–	Activity coefficient related to the mean adsorption energy, mol ² /J ²
b	–	Langmuir constant related to the adsorption energy, L/mg
b_T	–	Temkin model constant related to adsorption heat, J g/(mg mol)
C	–	Intra-particle diffusion model constant associated with the extent of boundary layer effect, mg/g
C_0	–	Initial concentration of the dye solution, mg/L
C_e	–	Equilibrium concentration of the dye solution, mg/L
C_s	–	Amount of the dye adsorbed per mass of adsorbent, mg/g
F	–	Fractional attainment of equilibrium
k_1	–	Pseudo-first-order rate parameter, min ⁻¹
k_2	–	Pseudo-second-order rate parameter, g/(mg min)
K_c	–	Adsorption equilibrium constant or distribution coefficient
K_f	–	Freundlich constants associated to the adsorption capacity, (mg/g) (L/mg) ^{1/n}
k_{fd}	–	Adsorption rate constant of liquid-film diffusion model, min ⁻¹
k_{id}	–	Intra-particle diffusion rate constant, mg/g min ^{-0.5}
n	–	Freundlich constants associated to adsorption intensity
q_e	–	Amount of the dye adsorbed on adsorbents at equilibrium, mg/g
q_m	–	Maximum adsorption capacity, mg/g
q_t	–	Amount of the dye adsorbed on adsorbents at time t , mg/g
R	–	Gas constant, J/(mol K)
T	–	Absolute temperature, K
t	–	Adsorption time, min
V	–	Volume of the dye solution, L
W	–	Weight of the adsorbent, g
α	–	Initial adsorption rate constant of Elovich model, mg/g min
β	–	Elovich model constant related to the surface coverage and the activation energy for chemical adsorption, g/mg
ΔG^0	–	Change of standard Gibbs free energy, kJ/mol
ΔH^0	–	Change of standard enthalpy, kJ/mol
ΔS^0	–	Change of standard entropy, J/(mol K)
E	–	Polanyi potential

Acknowledgments

This work was financially supported by the National Natural Science Foundation of China (529101–N11403).

The authors are extremely grateful to State Key Laboratory of Chemical Engineering (Zhejiang University, Hangzhou, China) for assistance of material characterizations, as well as to the anonymous referees and the editor for their helpful comments on the manuscript.

References

- [1] H.J. Hou, R.H. Zhou, P. Wu, L. Wu, Removal of Congo red dye from aqueous solution with hydroxyapatite/chitosan composite, *Chem. Eng. J.*, 211 (2012) 336–342.
- [2] R.P. Han, D.D. Ding, Y.F. Xu, W.H. Zou, Y.F. Wang, Y.F. Li, L. Zou, Use of rice husk for the adsorption of Congo red from aqueous solution in column mode, *Bioresour. Technol.*, 99 (2008) 2938–2946.
- [3] T. Feng, S. Xiong, F. Zhang, Application of cross-linked porous chitosan films for Congo red adsorption from aqueous solution, *Desal. Wat. Treat.*, 53 (2015) 1970–1976.
- [4] K.G. Bhattacharyya, A. Sharma, *Azadirachta indica* leaf powder as an effective biosorbent for dyes: a case study with aqueous Congo red solutions, *J. Environ. Manage.*, 71 (2004) 217–229.
- [5] A. Mittal, Retrospection of Bhopal gas tragedy, *Toxicol. Environ. Chem.*, 98 (2016) 1079–1083.
- [6] M.R. Gadekar, M.M. Ahammed, Coagulation/flocculation process for dye removal using water treatment residuals: modelling through artificial neural networks, *Desal. Wat. Treat.*, 57 (2016) 26392–26400.
- [7] P.S. Zhong, N. Widjojo, T.S. Chung, M. Weber, C. Maletzko, Positively charged nanofiltration (NF) membranes via UV grafting on sulfonated polyphenylenesulfone (sPPSU) for effective removal of textile dyes from wastewater, *J. Membr. Sci.*, 417 (2012) 52–60.
- [8] Y.L. Zhang, C.R. Xie, F.L. Gu, H.H. Wu, Q. Guo, Significant visible-light photocatalytic enhancement in rhodamine B degradation of silver orthophosphate via the hybridization of N-doped graphene and poly(3-hexylthiophene), *J. Hazard. Mater.*, 315 (2016) 23–34.
- [9] A.R. Khataee, G. Dehghan, A. Ebadi, M. Zarei, M. Pourhassan, Biological treatment of a dye solution by Macroalgae *Chara* sp.: effect of operational parameters, intermediates identification and artificial neural network modeling, *Bioresour. Technol.*, 101 (2010) 2252–2258.
- [10] M.T. Yagub, T.K. Sen, S. Afroze, H.M. Ang, Dye and its removal from aqueous solution by adsorption: a review, *Adv. Colloid Interface Sci.*, 209 (2014) 172–184.
- [11] R.R. Kalantri, A.J. Jafari, A. Esrafil, B. Kakavandi, A. Gholizadeh, A. Azari, Optimization and evaluation of reactive dye adsorption on magnetic composite of activated carbon and iron oxide, *Desal. Wat. Treat.*, 57 (2016) 6411–6422.
- [12] N.V. Suc, D.K. Chi, Removal of rhodamine B from aqueous solution via adsorption onto microwave-activated rice husk ash, *J. Dispersion Sci. Technol.*, 38 (2017) 216–222.
- [13] E. Ekrami, F. Dadashian, M. Arami, Adsorption of methylene blue by waste cotton activated carbon: equilibrium, kinetics, and thermodynamic studies, *Desal. Wat. Treat.*, 57 (2016) 7098–7108.
- [14] G. Sharma, M. Naushad, D. Pathania, A. Mittal, G.E. El-desoky, Modification of *Hibiscus cannabinus* fiber by graft copolymerization: application for dye removal, *Desal. Wat. Treat.*, 54 (2015) 3114–3121.
- [15] A. Mital, L. Kurup, Column operations for the removal and recovery of a hazardous dye 'Acid Red-27' from aqueous solutions using waste materials – bottom ash and de-oiled soya, *Ecol. Environ. Conserv.*, 12 (2006) 181–186.
- [16] A. Mittal, M. Teotia, R.K. Soni, J. Mittal, Applications of egg shell and egg shell membrane as adsorbents: a review, *J. Mol. Liq.*, 223 (2016) 376–387.
- [17] A. Mittal, J. Mittal, Hen Feather, a Remarkable Adsorbent for Dye Removal, S.K. Sharma, Ed., *Green Chemistry for Dyes Removal from Wastewater: Research Trends and Applications*, Scrivener Publishing LLC, USA, 2015, pp. 409–457.
- [18] N.P. Raval, P.U. Shah, D.G. Ladha, P.M. Wadhvani, N.K. Shah, Comparative study of chitin and chitosan beads for the adsorption of hazardous anionic azo dye Congo red from wastewater, *Desal. Wat. Treat.*, 57 (2016) 9247–9262.
- [19] A. Mittal, R. Ahmad, I. Hasan, Iron oxide-impregnated dextrin nanocomposite: synthesis and its application for the biosorption of Cr(VI) ions from aqueous solution, *Desal. Wat. Treat.*, 57 (2016) 15133–15145.
- [20] A. Mittal, R. Ahmad, I. Hasan, Biosorption of Pb²⁺, Ni²⁺ and Cu²⁺ ions from aqueous solutions by L-cystein-modified montmorillonite-immobilized alginate nanocomposite, *Desal. Wat. Treat.*, 57 (2016) 17790–17807.
- [21] A. Mittal, R. Ahmad, I. Hasan, Poly (methyl methacrylate)-grafted alginate/Fe₃O₄ nanocomposite: synthesis and its application for the removal of heavy metal ions, *Desal. Wat. Treat.*, 57 (2016) 19820–19833.
- [22] L.X. Zeng, Y.F. Chen, Q.Y. Zhang, Y. Kang, J.W. Luo, Adsorption of Congo red by cross-linked chitosan resins, *Desal. Wat. Treat.*, 52 (2014) 7733–7742.
- [23] W.S.W. Ngah, L.C. Teong, M.A.K.M. Hanafiah, Adsorption of dyes and heavy metal ions by chitosan composites: a review, *Carbohydr. Polym.*, 83 (2011) 1446–1456.
- [24] M. Auta, B.H. Hameed, Chitosan-clay composite as highly effective and low-cost adsorbent for batch and fixed-bed adsorption of methylene blue, *Chem. Eng. J.*, 237 (2014) 352–361.
- [25] H.M. Zhu, M.M. Zhang, Y.Q. Liu, L.J. Zhang, R.P. Han, Study of Congo red adsorption onto chitosan coated magnetic iron oxide in batch mode, *Desal. Wat. Treat.*, 37 (2012) 46–54.
- [26] T. Feng, F. Zhang, J. Wang, L. Wang, Application of chitosan-coated quartz sand for Congo red adsorption from aqueous solution, *J. Appl. Polym. Sci.*, 125 (2012) 1766–1772.
- [27] L. Wang, A.Q. Wang, Removal of Congo red from aqueous solution using a chitosan/organo-montmorillonite nanocomposite, *J. Chem. Technol. Biotechnol.*, 82 (2007) 711–720.
- [28] H.Y. Li, Y.Q. Tan, L. Zhang, Y.X. Zhang, Y.H. Song, Y. Ye, M.S. Xia, Bio-filler from waste shellfish shell: preparation, characterization, and its effect on the mechanical properties on polypropylene composites, *J. Hazard. Mater.*, 217 (2012) 256–262.
- [29] S. Sudo, T. Fujikawa, T. Nagakura, T. Ohkubo, K. Sakaguchi, M. Tanaka, K. Nakashima, T. Takahashi, Structures of mollusc shell framework proteins, *Nature*, 387 (1997) 563–564.
- [30] Z.T. Yao, T. Chen, H.Y. Li, M.S. Xia, Y. Ye, H. Zheng, Mechanical and thermal properties of polypropylene (PP) composites filled with modified shell waste, *J. Hazard. Mater.*, 262 (2013) 212–217.
- [31] L.Q. Ge, W.Y. Yang, H. Lv, M.S. Xia, X.S. Ji, Z.T. Yao, Colorating and mechanical performance of low-density polyethylene (LDPE)/dye-loaded shell powder (DPSP) composites, *Fibers Polym.*, 16 (2015) 1294–1302.
- [32] Z.T. Yao, M.S. Xia, H.Y. Li, T. Chen, Y. Ye, H. Zheng, Bivalve shell: not an abundant useless waste but a functional and versatile biomaterial, *Crit. Rev. Environ. Sci. Technol.*, 44 (2014) 2502–2530.
- [33] S.D. Cifrolak, High pressure mid-infrared studies of calcium carbonate, *Am. Mineral.*, 55 (1970) 815–824.
- [34] C.Y. Lin, S.X. Li, M. Chen, R. Jiang, Removal of Congo red dye by gemini surfactant C-12-4–C-12 center dot 2Br-modified chitosan hydrogel beads, *J. Dispersion Sci. Technol.*, 38 (2017) 46–57.
- [35] B. Van Raij, M. Peech, Electrochemical properties of some oxisols and alfisols of the tropics, *Soil Sci. Soc. Am. J.*, 36 (1972) 587–593.
- [36] G. Uehara, G. Gillman, *The Mineralogy, Chemistry, and Physics of Tropical Soils with Variable Charge Clays*, Westview Press Inc., Boulder, 1981.
- [37] R.H. Huang, L.J. Zhang, P. Hu, J. Wang, Adsorptive removal of Congo red from aqueous solutions using crosslinked chitosan and crosslinked chitosan immobilized bentonite, *Int. J. Biol. Macromol.*, 86 (2016) 496–504.
- [38] S. Lagergren, About the theory of so-called adsorption of soluble substances, *K. Sven. Vetensk.akad. Handl.*, 24 (1898) 1–39.

- [39] Y.S. Ho, G. McKay, Sorption of dye from aqueous solution by peat, *Chem. Eng. J.*, 70 (1998) 115–124.
- [40] G.E. Boyd, A.W. Adamson, L.S. Myers, The exchange adsorption of ions from aqueous solutions by organic zeolites, *J. Am. Chem. Soc.*, 69 (1947) 2836–2848.
- [41] S.H. Chien, W.R. Clayton, Application of Elovich equation to the kinetics of phosphate release and sorption in soils, *Soil Sci. Soc. Am. J.*, 44 (1980) 265–268.
- [42] W.J. Weber, J.C. Morris, Kinetics of adsorption on carbon from solution, *J. Sanit. Eng. Div.*, 89 (1963) 31–60.
- [43] Y.S. Ho, G. McKay, A comparison of chemisorption kinetic models applied to pollutant removal on various sorbents, *Process Saf. Environ. Prot.*, 76 (1998) 332–340.
- [44] G.L. Dotto, L.A.A. Pinto, Adsorption of food dyes onto chitosan: optimization process and kinetic, *Carbohydr. Polym.*, 84 (2011) 231–238.
- [45] S. Thakur, S. Pandey, O.A. Arotiba, Development of a sodium alginate-based organic/inorganic superabsorbent composite hydrogel for adsorption of methylene blue, *Carbohydr. Polym.*, 153 (2016) 34–46.
- [46] N. Chen, Z.Y. Zhang, C.P. Feng, D.R. Zhu, Y.N. Yang, N. Sugiura, Preparation and characterization of porous granular ceramic containing dispersed aluminum and iron oxides as adsorbents for fluoride removal from aqueous solution, *J. Hazard. Mater.*, 186 (2011) 863–868.
- [47] I. Langmuir, The adsorption of gases on plane surfaces of glass, mica and platinum., *J. Am. Chem. Soc.*, 40 (1918) 1361–1403.
- [48] H.M.F. Freundlich, Über die adsorption in losungen, *Int. J. Res. Phys. Chem. Chem. Phys.*, 57 (1906) 385–470.
- [49] M.I. Temkin, Adsorption equilibrium and process kinetics on nonhomogenous surface with interaction between adsorbed molecules, *Zh. Fiz. Khim.*, 15 (1941) 296–332.
- [50] M.M. Dubinin, L.V. Radushkevich, Equation of the characteristics curve of activated charcoal, *Chem. Zentralbl.*, 1 (1947) 875–889.
- [51] N.T. Abdel-Ghani, E.S.A. Rawash, G.A. El-Chaghaby, Equilibrium and kinetic study for the adsorption of p-nitrophenol from wastewater using olive cake based activated carbon, *Global J. Environ. Sci.*, 2 (2016) 11–18.
- [52] Q.J. Du, J.K. Sun, Y.H. Li, X.X. Yang, X.H. Wang, Z.H. Wang, L.H. Xia, Highly enhanced adsorption of Congo red onto graphene oxide/chitosan fibers by wet-chemical etching off silica nanoparticles, *Chem. Eng. J.*, 245 (2014) 99–106.
- [53] L. Wang, A.Q. Wang, Adsorption characteristics of Congo red onto the chitelsan/montmorillonite nanocomposite, *J. Hazard. Mater.*, 147 (2007) 979–985.
- [54] S. Chatterjee, M.W. Lee, S.H. Woo, Adsorption of Congo red by chitosan hydrogel beads impregnated with carbon nanotubes, *Bioresour. Technol.*, 101 (2010) 1800–1806.
- [55] Q.Y. Zhang, M.J. Xie, X.M. Guo, L.X. Zeng, J.W. Luo, Fabrication and adsorption behavior for Congo red of chitosan and alginate sponge, *Integr. Ferroelectr.*, 151 (2014) 61–75.
- [56] P.S. Kumar, S. Ramalingam, C. Senthamarai, M. Niranjanaa, P. Vijayalakshmi, S. Sivanesan, Adsorption of dye from aqueous solution by cashew nut shell: studies on equilibrium isotherm, kinetics and thermodynamics of interactions, *Desalination*, 261 (2010) 52–60.